MANNOSE RECEPTOR DEFICIENCY PROTECTS AGAINST HIGH-FAT DIET-INDUCED INSULIN RESISTANCE AND DECREASES CLASSICAL ACTIVATION OF LIVER AND ADIPOSE TISSUE MACROPHAGES

Leonie Hussaarts, Noemí García-Tardón, Simone Haeberlein, Karin de Ruiter, Lisa Hoving, Arifa Ozir-Fazalalikhan, Gerard C. van der Zon, Vanessa van Harmelen, Sven Burgdorf, Maria Yazdanbakhsh and Bruno Guigas

6

Manuscript in preparation

ABSTRACT

Chronic low-grade inflammation associated with obesity is one of the major contributors to insulin resistance, enhancing the risk for type 2 diabetes and cardiovascular diseases. The mannose receptor (MR) is an endocytic C-type lectin receptor predominantly expressed by dendritic cells and macrophages, including alternatively activated M2 macrophages that protect against insulin resistance. To investigate the role of MR on whole-body metabolic homeostasis, wild-type (WT) and MR knockout ($MR^{-/-}$) mice were studied following 18 weeks of low-fat diet (LFD) or high-fat diet (HFD). Although no metabolic phenotype was observed in LFD-fed $MR^{-/-}$ mice, on HFD we found significant reductions in total body weight (-8.3%), fat mass gain (-25.6%), and liver weight (-16.6%) compared to WT mice. Furthermore, MR deficiency lowered HFD-induced alterations in both whole-body glucose tolerance and insulin sensitivity (-22.9% and -17.1%, respectively), as assessed by intraperitoneal glucose and insulin tests. This effect was associated with enhanced locomotor activity, food intake and energy expenditure in $MR^{-/-}$ mice when compared to WT. Remarkably, analysis of the immune cell composition of metabolic organs indicated that HFD decreased white adipose tissue (WAT) eosinophil numbers in WT but not $MR^{-/-}$ mice. In addition, $MR^{-/-}$ mice were less susceptible to HFD-induced classical activation of macrophages, in both WAT and liver. In conclusion, we show that whole-body MR deficiency lowers HFD-induced chronic low grade inflammation of metabolic tissues and protects against insulin resistance in obese mice, suggesting that MR might play an unexpected role in the development of metabolic disorders.

INTRODUCTION

The mannose receptor (MR, CD206) is an endocytic C-type lectin receptor implicated in binding of glycoproteins from endogenous and microbial origin, and in antigen presentation (1). Over the past decade, it has become clear that the MR may play a pivotal role in regulating type 2 inflammatory responses. For example, MR is required for Th2 polarization by human monocyte-derived dendritic cells stimulated with helminth antigens (2) and Der p 1 allergen (3). In line with these findings, lack of MR was shown to promote Th1 cytokine production following *Schistosoma mansoni* infection (4), and to reduce IgE production in response to allergen sensitization (5). Furthermore, MR-deficient mice exhibit defective clearance of endogenous serum glycoproteins (6), and it was recently described that MR expression by macrophages mediates collagen uptake (7), suggesting that the receptor may also contribute to tissue repair and remodeling.

MR is predominantly expressed by subpopulations of dendritic cells and macrophages, including microglial cells (8;9), although its expression is not only restricted to leukocytes. For example, in mice, MR is also expressed by hepatic, splenic, lymphatic and dermal microvascular endothelia, and by glomerular kidney mesangial cells, tracheal smooth muscle cells, and retinal pigment epithelium (1;9;10). Macrophage subpopulations are traditionally classified along a linear scale, on which pro-inflammatory M1 macrophages represent one extreme, and alternatively activated M2 macrophages the other (11). While classical activation of macrophages depends on T helper 1-associated cytokines like IFN-γ (12;13), M2-like activation is mediated by type 2 cytokines, like IL-4 and IL-13, which concomitantly promote upregulation of MR expression (14;15).

While accumulation of TNF-α-secreting M1 macrophages has been reported in both liver and white adipose tissue (WAT) of obese mice, M2 macrophages prevail in lean adipose tissue and liver (16-19), where they can mediate energy homeostasis via multiple routes. WAT M2 macrophages were shown to secrete IL-10, which can act directly on adipocytes to potentiate insulin signaling and therefore inhibit TNF-α-induced insulin resistance (18;20). In addition, M2 macrophages mediate tissue repair (reviewed in (21)) and regulate thermogenesis by promoting biogenesis of beige fat in response to cold (22;23). In liver, M2-like Kupffer cells were suggested to directly modulate hepatic metabolism in favor of β-oxidation and mitochondrial oxidative phosphorylation (16). The M2 phenotype is sustained by cells that secrete type 2 cytokines, like eosinophils (24) and type 2 innate lymphoid cells (25), which thereby also contribute to metabolic homeostasis.

Although expression of MR is a hallmark of the M2 phenotype (14), and a close link has been described between MR and type 2 inflammation, the role of the MR in metabolic homeostasis remains unclear. In the present study, we therefore studied whole-body insulin sensitivity and glucose homeostasis, and immune cell polarization in metabolic organs from wild-type (WT) and MR-deficient mice ($MR^{-/-}$) fed a low-fat diet (LFD) or high-fat diet (HFD). We report that $MR^{-/-}$ mice are less susceptible to HFD-induced obesity, insulin resistance and inflammation of metabolic tissues than WT mice, suggesting that the MR plays an unexpected role in the development of HFD-induced metabolic disorders.

RESULTS

MR deficiency protects against HFD-induced obesity

Before being put on LFD or HFD, three-month-old WT and MR$^{-/-}$ mice were similar in terms of body weight, lean mass, fat mass, and fasting plasma glucose and triglyceride levels (Table S1). However, MR$^{-/-}$ mice had slightly higher fasting plasma cholesterol levels, and a trend for lower insulin levels (Table S1). To investigate the impact of MR deficiency on whole-body energy and metabolic homeostasis, C57BL/6 WT and MR$^{-/-}$ mice were fed a LFD or HFD for 18 weeks. As expected, HFD induced an increase in body weight (Fig. 1A) and fat mass (Fig. 1B)

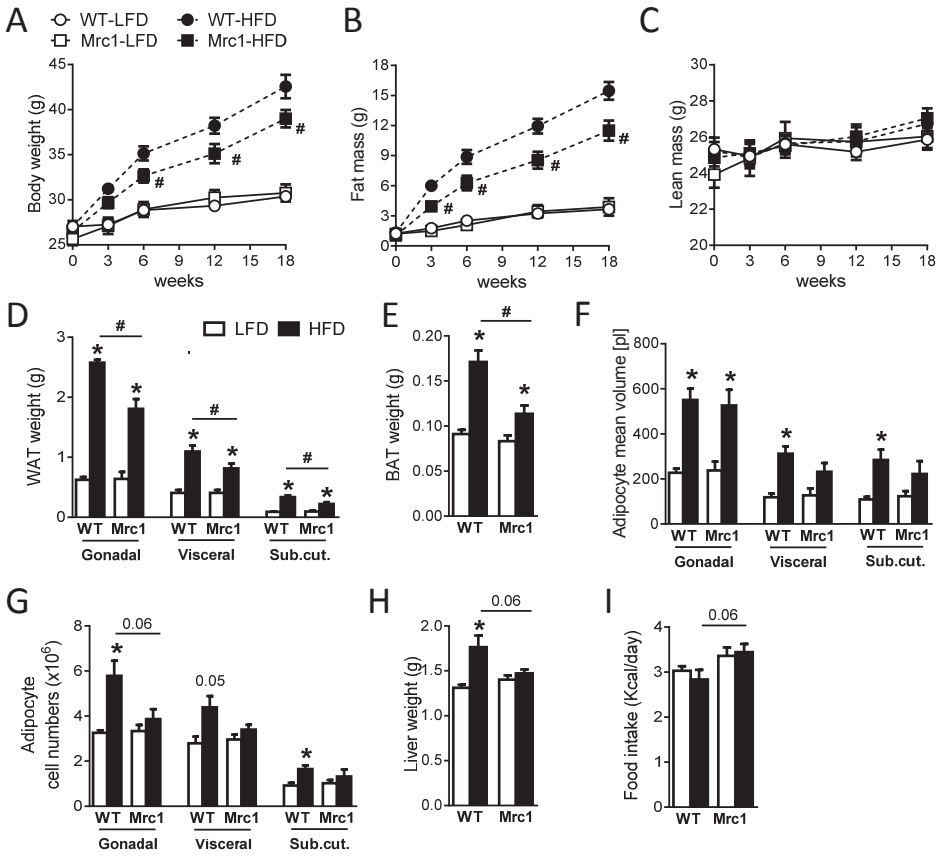

Figure 1. MR deficiency protects against HFD-induced weight gain, fat mass gain and adipocyte hyperplasia. Wild-type (WT) and MR-deficient (Mrc1) mice were fed a LFD or a HFD for 18 weeks. Throughout the experimental period, body weight (A) and body composition were monitored, and fat mass (B) and lean mass (C) were determined. At sacrifice, the weight of the different white fat pads (D) and of the subcutaneous brown fat (E) were measured, as well as the adipocyte mean volume (F) and the number of adipocytes (G). Liver weight was determined at sacrifice (H), and food intake was assessed using fully automated single-housed metabolic cages at week 16 (I). Results are expressed as means ± SEM. * P<0.05 HFD *vs* LFD, # P<0.05 WT *vs* Mrc1 (n = 10-15 animals per group in A-E,H, and 4-8 animals per group in F,G,I).

without affecting lean mass (Fig. 1C) in both WT and $MR^{-/-}$ mice. However, $MR^{-/-}$ mice gained significantly less body weight than WT mice (Fig. 1A), secondary to a decrease in fat mass gain (Fig. 1B). Analysis of the individual fat pads showed that MR deficiency impaired HFD-induced weight gain of WAT (Fig. 1D) and brown adipose tissue (Fig. 1E). White adipocyte volume was not significantly different between genotypes (Fig. 1F), but the number of adipocyte cells was lower in HFD-fed $MR^{-/-}$ when compared to WT mice (Fig. 1G). MR deficiency also impaired HFD-induced gain of liver mass (Fig. 1H), suggesting a reduction in hepatic steatosis. Importantly, the effects of MR deficiency on body composition were not due to a decrease in food consumption, since lack of MR was rather accompanied by a mild increase in caloric intake (Fig. 1I).

Furthermore, HFD reduced locomotor activity (Fig. 2A) and energy expenditure (EE; Fig. 2B) in WT mice, but not in $MR^{-/-}$ mice. In both genotypes, HFD reduced carbohydrate oxidation (CHO; Fig. 2C) and increased fatty acid oxidation (FAO; Fig. 2D), although $MR^{-/-}$ mice were found to oxidize slightly more carbohydrates (Fig. 2C). Taken together, these findings show that $MR^{-/-}$ mice are partly protected against HFD-induced obesity, an effect associated with increased locomotor activity, food intake and energy expenditure.

MR deficiency improves whole-body glucose tolerance and insulin sensitivity in HFD-fed mice

We next investigated the effect of MR deficiency on fasting plasma parameters in LFD- and HFD-fed mice. In both genotypes, HFD increased plasma glucose (Fig. 3A) and insulin levels (Fig. 3B), HOMA-IR (Fig. 3C), and total cholesterol (Fig. 3D), without affecting triglyceride levels (Fig. 3E). However, lack of MR significantly decreased the HFD-induced rise in plasma insulin levels (Fig. 3B) and improved HOMA-IR (Fig. 3C), suggesting a lower insulin resistance than WT mice. In line with these findings, HFD-fed $MR^{-/-}$ mice exhibited a better glucose tolerance, as assessed by an intraperitoneal glucose tolerance test (ipGTT Fig. 3F), without a change in insulin levels (Fig. 3G), indicating improvement in whole-body insulin sensitivity. This was confirmed by an intraperitoneal insulin tolerance test (ipITT) showing that acute injection of insulin lowered glucose levels to a larger extent in $MR^{-/-}$ mice compared to WT mice (Fig. 3H). Taken together, these findings suggest that $MR^{-/-}$ mice are less susceptible to HFD-induced metabolic dysfunctions than WT mice.

MR deficiency attenuates HFD-induced inflammation in adipose tissue

Based on the finding that M2 macrophages protect against insulin resistance (26), and the association between the MR and the M2 phenotype (14), we next investigated whether MR deficiency affects adipose tissue inflammation. We isolated the stromal vascular fraction (SVF) from gonadal WAT and analyzed the immune cell composition by flow cytometry. Analysis of myeloid cells (Fig. 4A) indicated that HFD reduced the numbers of eosinophils (Fig. 4B) and neutrophils (Fig. 4C) only in WT mice and not in $MR^{-/-}$ mice. Furthermore, HFD increased the number of M1 macrophages in WT mice (Fig. 4D), thereby decreasing the M2/M1 ratio (Fig. 4E), as expected. Remarkably, while total macrophage numbers were not affected by diet

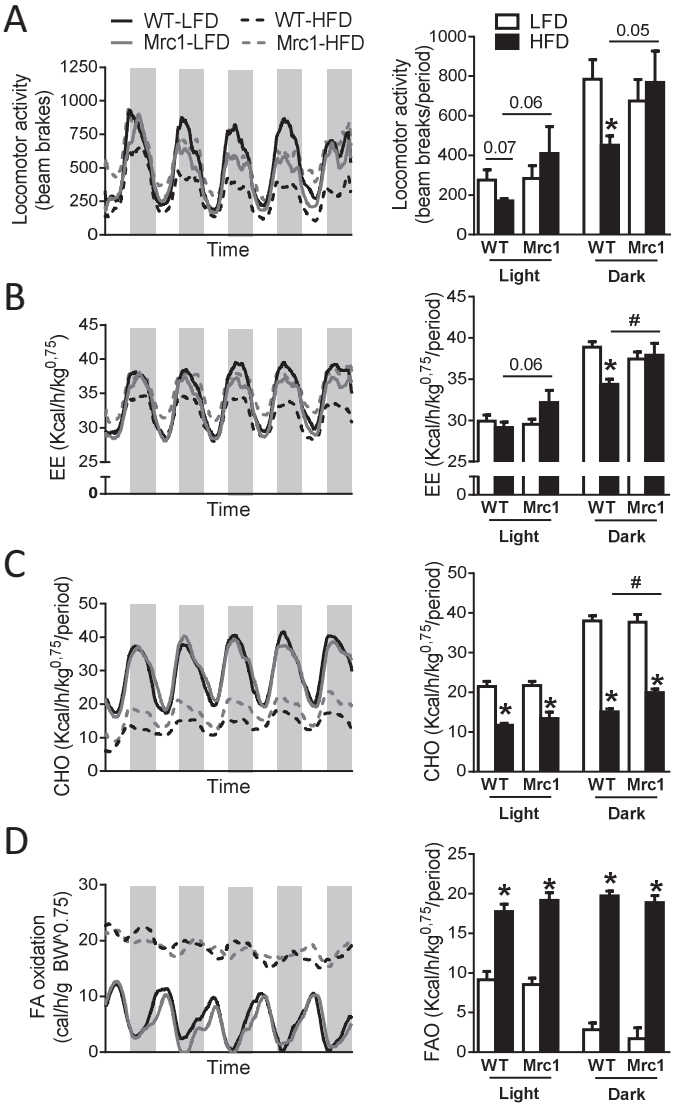

Figure 2. HFD does not affect locomotor activity and energy expenditure in MR$^{-/-}$ mice. Wild-type (WT) and MR-deficient (Mrc1) mice were fed a LFD or a HFD for 18 weeks. At week 16, mice with free access to food and water were subjected to individual indirect calorimetric measurements using fully automated metabolic cages. Spontaneous locomotor activity (A), energy expenditure (EE; B), carbohydrate oxidation (CHO; C) and fatty acid oxidation (FAO; D) were determined. Results are expressed as means ± SEM. * P<0.05 HFD *vs* LFD, # P<0.05 WT *vs* Mrc1 (n = 6-8 animals per group).

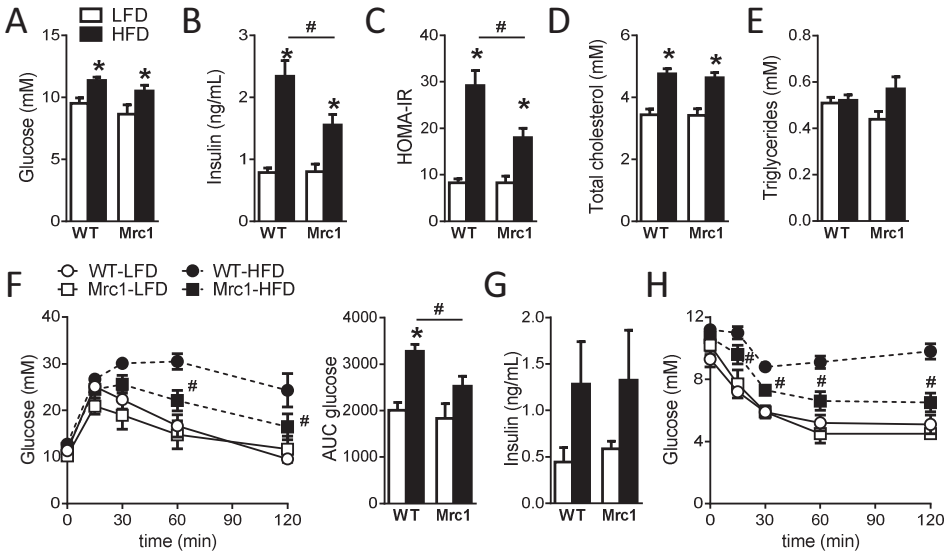

Figure 3. MR deficiency improves whole-body glucose tolerance and insulin sensitivity in HFD-fed animals. Wild-type (WT) and MR-deficient (Mrc1) mice were fed a LFD or a HFD for 18 weeks. At week 18, mice were fasted for 4h and plasma was collected to determine glucose (A) and insulin levels (B), HOMA-IR (C), and total cholesterol (D) and triglyceride levels (E). An intravenous glucose tolerance test (2g D-glucose/kg body weight) was performed in 6h-fasted mice at week 17. Blood glucose levels were measured at the indicated time points and the area under the curve (AUC) of the glucose excursion curve was calculated as a measure for glucose tolerance (F). 15 minutes after the i.p. bolus of glucose, blood was also collected for analysis of plasma insulin levels (G). An i.p. insulin tolerance test (1U/kg lean body mass) was performed in 4h-fasted mice at week 15. Blood glucose levels were measured at the indicated time points (H). Results are expressed as means ± SEM. * P<0.05 HFD *vs* LFD, # P<0.05 WT *vs* Mrc1. Figures F, and H: only statistical significance of HFD WT *vs* HFD Mrc1 is shown (n = 10-15 animals per group in A-E, and 3-10 animals per group in F-H).

or genotype (Fig. 4E), MR-deficient mice had higher numbers of M2 macrophages, and were partly protected against HFD-induced M1 polarization (Fig. 4F). As a consequence, HFD did not alter the M2/M1 ratio in $MR^{-/-}$ mice (Fig. 4G). These findings were confirmed by quantitative PCR (qPCR), which indicated that lack of MR reversed HFD-induced increases in gene expression levels of *Itgax* (encoding CD11c), and the chemokine receptor *Ccr2* (Fig. S1A). Interestingly, neither diet nor genotype affected the numbers of eosinophils, neutrophils and inflammatory monocytes in the blood (Fig. S2), suggesting that the observed changes in myeloid immune cell composition are adipose tissue-specific.

Cells that secrete type 2 cytokines were shown to promote alternative activation of macrophages (13). Therefore, T cell and ILC responses in WAT of HFD-fed mice were analyzed next (Fig. 4G). MR deficiency significantly increased the frequency of ILCs, but not $CD4^+$ T cells (Fig. 4H). Analysis of cytokine expression following *ex vivo* stimulation with phorbol myristate acetate (PMA) and ionomycin showed that IL-13 expression by WAT $CD4^+$ T cells and ILCs was not significantly different between genotypes (Fig. 4I). We confirmed these findings by qPCR,

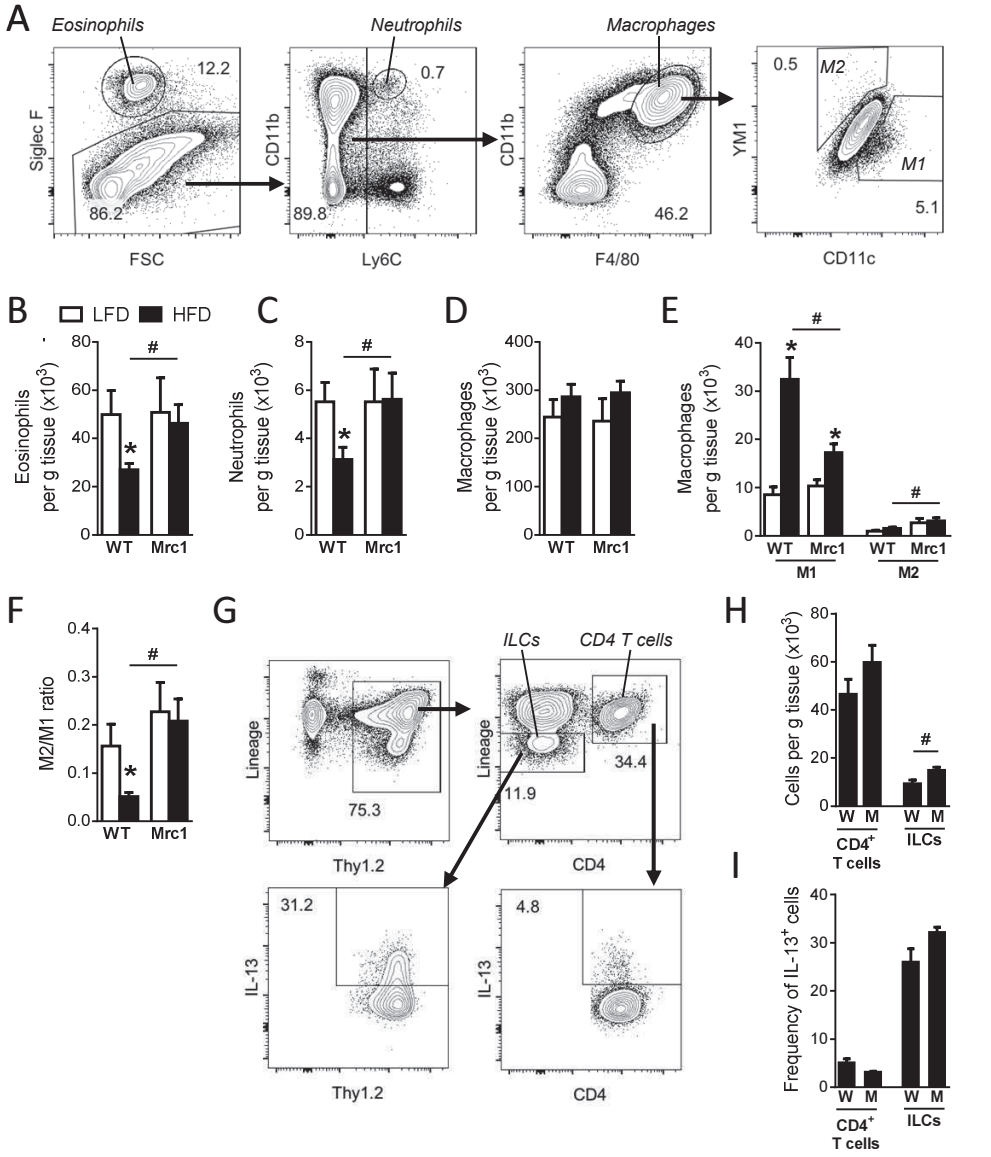

Figure 4. MR-deficient mice are less sensitive to HFD-induced inflammation in adipose tissue. Wild-type (WT) and MR-deficient (Mrc1) mice were fed a LFD or a HFD for 18 weeks. At sacrifice, gonadal adipose tissue was collected and the stromal vascular fraction (SVF) was isolated. Following fixation and permeabilization, SVF cells were stained and analyzed by flow cytometry. Cells were pre-gated for Aqua$^-$ CD45$^+$ single cells. The gating strategy is shown for eosinophils, neutrophils, CD11c$^+$ M1 macrophages and YM1$^+$ M2 macrophages (A). The numbers of eosinophils (B), neutrophils (C), total macrophages (D) and M1 and M2 macrophages (E) per gram WAT were determined and the M2/M1 ratio was calculated (F). Following gating on Aqua$^-$CD45$^+$ single cells, lymphocyte subsets were analyzed by selecting for Thy1.2$^+$ cells to enrich for T cells and ILCs. T cells were subsequently identified as Lineage$^+$CD4$^+$ cells, in which the lineage cocktail included antibodies against CD3, CD11b, CD11c, B220, GR-1, and NK1.1. ILCs were identified ▶

which indicated that expression of pro- and anti-inflammatory cytokines was largely similar between groups (Fig. S1A).

MR deficiency attenuates HFD-induced activation of Kupffer cells

Obesity has also been associated with classical activation of liver macrophages (19). Therefore, $CD45^+$ cells were isolated from liver and the hepatic immune cell composition was studied. Analysis of myeloid cells (Fig. 5A) showed that neither HFD nor genotype affected the numbers of eosinophils (Fig. 5B), neutrophils (Fig. 5C), monocytes (not shown), or $CD45^+SiglecF^-CD11b^{lo}F4/80^{hi}$ macrophages (Fig. 5D), which were previously identified as Kupffer cells (27). Although we did not observe an effect of diet or genotype on YM1 expression by Kupffer cells, HFD significantly increased the expression of CD11c by these cells in WT mice, as expected (19). Remarkably, CD11c expression by Kupffer cells from $MR^{-/-}$ mice was not affected by HFD-feeding (Fig. 5E). These findings were confirmed and expanded by qPCR analysis, which showed that HFD-feeding induced expression of *Itgax, Nos2, Ccl2 and Ccr2* in WT but not $MR^{-/-}$ mice (Fig. S1B).

Analysis of cytokine responses (Fig. 5F) indicated that HFD reduced the frequency of type 2 cytokine-expressing $CD4^+$ T cells (Fig. 5G) and ILCs (Fig. 5H) in the livers of WT mice. Furthermore, expression of the ILC2-associated marker ICOS was decreased as a consequence of HFD (Fig. 5I). Although not significant, similar trends were observed for $MR^{-/-}$ mice fed a HFD. These findings were confirmed by qPCR (Fig. S1B). Taken together, the results indicate that MR deficiency reduces susceptibility to HFD-induced classical activation of macrophages, in both WAT and liver.

DISCUSSION

Alternatively activated M2 macrophages prevail in lean adipose tissue and protect against diet-induced metabolic disorders (26). Because the MR is highly expressed by M2 macrophages (14), we explored the role the MR in the context of diet-induced obesity using $MR^{-/-}$ mice. We report that lack of MR did not affect whole-body glucose tolerance and insulin sensitivity in mice fed a LFD, but counterintuitively improved metabolic homeostasis in mice fed a HFD despite considerable weight gain. Specifically, $MR^{-/-}$ mice on HFD were less susceptible to fat mass gain and adipocyte hyperplasia, had a higher locomotor activity, and showed better insulin sensitivity and glucose tolerance than WT mice on HFD. Immune profiling indicated that in line with their metabolic phenotype, MR-deficient mice were less sensitive to HFD-induced classical activation of M1-like macrophages, in both liver and adipose tissue. Furthermore, in WAT, HFD reduced eosinophil and neutrophil numbers in WT but not $MR^{-/-}$ mice. Contrary to expectations,

as $Lineage^-CD4^-$ cells (G). The numbers of $CD4^+$ T cells and ILCs per gram WAT were determined (H). Intracellular IL-13 expression was analyzed after 4h stimulation with PMA and ionomycin in the presence of Brefeldin A, the frequencies of $IL\text{-}13^+$ $CD4^+$ T cells and the frequencies of $IL\text{-}13^+$ ILCs are shown (I). Results are expressed as means ± SEM. * $P<0.05$ HFD *vs* LFD, # $P<0.05$ WT *vs* Mrc1 (n = 10-15 animals per group in A-F, and 5-10 animals per group in G-I).

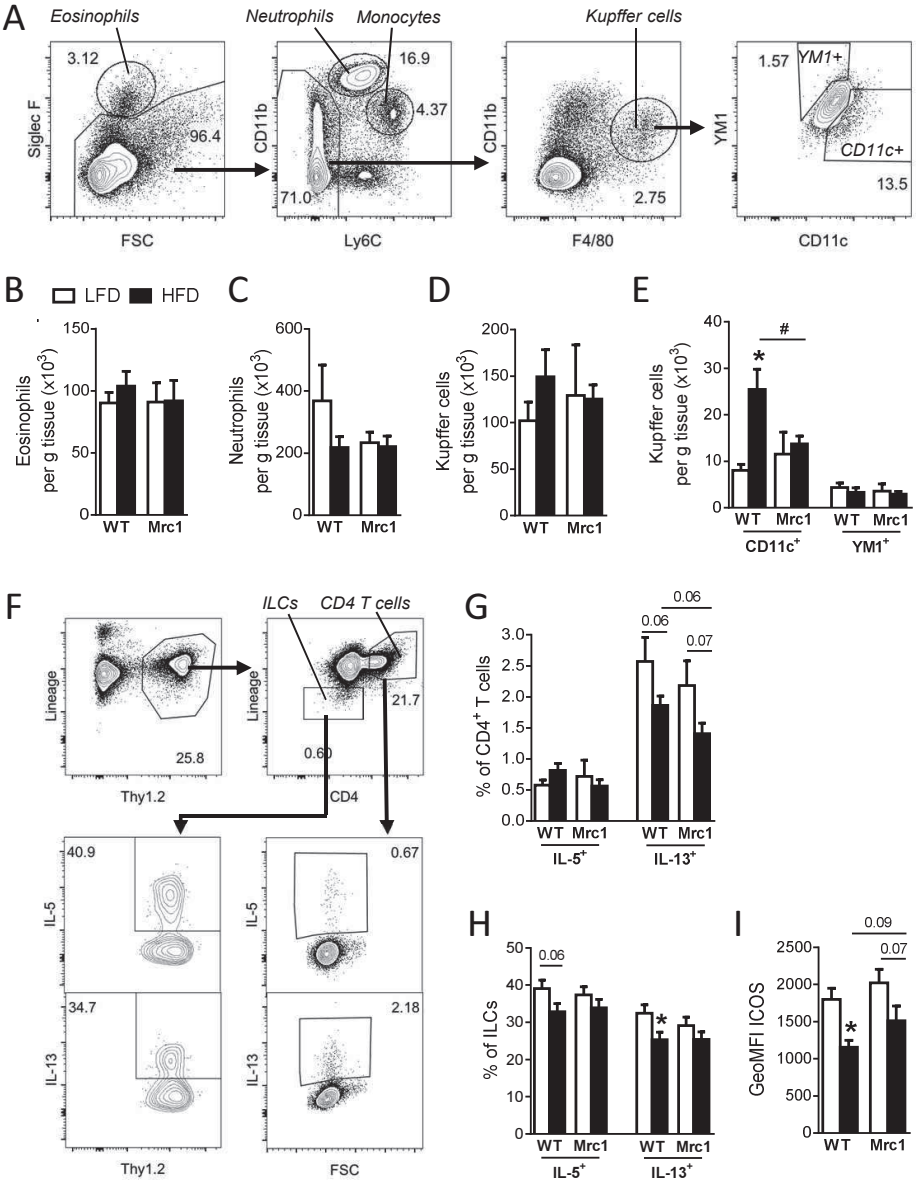

Figure 5. MR-deficient mice are less sensitive to HFD-induced activation of Kupffer cells. Wild-type (WT) and MR-deficient (Mrc1) mice were fed a LFD or a HFD for 18 weeks. At sacrifice, CD45$^+$ liver cells were isolated and analyzed by flow cytometry as described in the legend of Figure 4. The gating strategy is shown for eosinophils, neutrophils, CD11c$^+$ Kupffer cells and YM1$^+$ Kupffer cells (A). The numbers of eosinophils (B), neutrophils (C), Kupffer cells (D), and CD11c$^+$ and YM1$^+$ Kupffer cells (E) per gram of liver tissue were determined. Intracellular cytokine expression was analyzed after 4h stimulation with PMA and ionomycin in the presence of Brefeldin A. The gating strategy, as described in the legend of Figure 4, is shown for CD4$^+$ T cells and ILCs (F). The frequencies of IL-5$^+$ and IL-13$^+$ CD4$^+$ T cells (G) and IL-5$^+$ and IL-13$^+$ ILCs (H) are shown, and the expression of ICOS by ILCs was analyzed (H). Results are expressed as means ± SEM. * P<0.05 HFD *vs* LFD, # P<0.05 WT *vs* Mrc1 (n = 10-15 animals per group).

M2-like activation and type 2-associated cytokine expression by T helper cells and ILC2s were not as strongly affected by genotype. These effects were surprising, given the association between MR and the M2 phenotype (14), and the pivotal role MR plays in the initiation of type 2 immune responses (2-5). The question whether immune- on non-immune-mediated mechanisms promote metabolic health in MR-deficient obese mice needs to be addressed.

We observed that MR-deficient mice are less susceptible to HFD-induced classical activation of macrophages. A possible immune-based explanation may be provided by our finding that M1 macrophages can also express MR, albeit to a much lower extent than M2 macrophages (unpublished data). In this context, it is worth mentioning that macrophage-associated scavenger receptors have been described to promote either pro- or anti-inflammatory responses depending on the co-receptor they form complexes with (28), and it has been suggested that the MR can form complexes with other receptors (29). Taken together, these observations may indicate that the MR can deliver a signal directly into the MR-bearing macrophage, which may result in polarization of either pro- or anti-inflammatory macrophages, depending on the nature of the co-receptors. Future studies are needed to elucidate whether MR expression by macrophages indeed mediates a pro-inflammatory phenotype under HFD conditions.

It is important to consider that $MR^{-/-}$ mice lack whole-body expression of the *Mrc1* gene. In the mouse adult brain, MR is expressed by microglia and astrocytes, although its activities and involvement in brain functions are largely unknown (30). Of note, hypothalamic inflammation has been described to contribute to HFD-induced weight gain by promoting accumulation of microglia and astrocytes in various regions of the hypothalamus that coordinate the regulation of peripheral nutrient metabolism and energy expenditure (31;32). To study whether neuroinflammation differs between WT and $MR^{-/-}$ mice, we performed qPCR analysis on whole hypothalamus. Although we observed the classical HFD-induced increase in some markers of inflammation, we did not find significant effects of genotype on expression of inflammatory genes (not shown). Recent literature suggested that the brain can also regulate metabolic homeostasis through the cholinergic anti-inflammatory reflex. In this reflex, molecular products of inflammation promote the release of acetylcholine by the *vagus* nerve, which reduces inflammation (33). It was recently demonstrated that neuronal deletion of *Pten*, a negative regulator of the PI3K pathway, activates the anti-inflammatory reflex, which promotes WAT M2 polarization and protects against insulin resistance in mice on HFD (34). The question whether MR deficiency affects HFD-induced neuroinflammation and/or activation of the anti-inflammatory reflex, and the possible consequences for metabolic disorders, remains an intriguing area of research.

MR expression is not only restricted to leukocytes (1), and the beneficial effect of MR deficiency on metabolic homeostasis might therefore be due to effects beyond the immune system or the brain. For example, high-fat diet-feeding increases LPS translocation from the gut (35), and it has been suggested that this so-called metabolic endotoxemia can contribute to M1 polarization in WAT (36). It would therefore be important to establish whether lack of MR affects LPS translocation and its circulating plasma level in response to HFD. Furthermore, MR on lymphatics is required for lymphocyte trafficking from the periphery into the draining

lymph nodes (37). MR deficiency may therefore prevent the induction of a strong immune response to HFD-feeding. Lastly, MR can also be expressed by cells in metabolic organs where it can play a functional role. Expression of MR by liver sinusoidal endothelial cells has been associated with clearance of lysosomal enzymes and collagen (6;38;39), and it was suggested that MR is required for the growth of skeletal muscle myofibers (40). We did not observe a metabolic phenotype in the LFD-fed $MR^{-/-}$ animals, but we cannot exclude the possibility that expression of MR in metabolic tissues may mediate insulin resistance when the system is triggered by HFD-feeding.

In conclusion, our work has revealed an unexpected role for the MR in the development of obesity-induced metabolic disorders. Contrary to expectations, we have established that $MR^{-/-}$ mice are less susceptible to HFD-induced weight gain, insulin resistance and glucose intolerance. These effects were associated with increased locomotor activity and energy expenditure, and decreased classical activation of WAT and liver macrophages. Whether the protective effect of MR deficiency can be attributed to MR expression by immune or non-immune cells remains an important area of research. Understanding these processes may offer valuable insights towards the development of targeted therapeutics for the treatment of metabolic syndrome.

MATERIALS AND METHODS

Animals and diet

All experiments were performed in accordance with the Guide for the Care and Use of Laboratory Animals of the Institute for Laboratory Animal Research and have received approval from the university Ethical Review Boards (Leiden University Medical Center, Leiden, The Netherlands). Male $MR^{-/-}$ mice on a CD57BL/6 background, generated as described previously (6), were provided by Dr. Sven Burgdorf (University of Bonn, Germany). $MR^{-/-}$ mice and age-matched C57BL/6 WT mice from the same breeding facility were housed in a temperature-controlled room with a 12 hour light-dark cycle. Throughout the experiment, food and tap water were available *ad libitum*. 8 – 10 week old mice were randomized according to total body weight, lean and fat mass, and fasting plasma glucose, insulin, TC and TG levels, after which they were fed a high-fat diet (HFD, 45% energy derived from fat, D12451, Research Diets) or a low-fat diet (LFD, 10% energy derived from fat, D12450B, Research Diets) for 18 weeks. Diets were similar in composition in all respects apart from the total fat content.

Plasma analysis

Blood samples were collected at 1:00 pm using chilled paraoxon-coated capillaries from the tail tip of 4h-fasted mice 18 weeks after the start of LFD- or HFD-feeding. Blood glucose level was determined using a Glucometer (Accu-Check, Roche Diagnostics). Using commercially available kits and standards according to the instructions of the manufacturer, we determined total cholesterol and triglycerides (Instruchemie) and plasma insulin (Chrystal Chem).

Glucose and insulin tolerance tests

Glucose tolerance was assessed by an ipGTT 17 weeks after the start of LFD- or HFD-feeding. Mice were fasted for 6h, and the tests were carried out at 2:00 pm. After an initial blood collection (t=0), an i.p. injection of glucose (2g D-Glucose/kg total body weight, Sigma-Aldrich) was administered in conscious mice. Blood glucose was measured by tail bleeding at 15, 30, 60, 90 and 120 minutes after glucose administration using a Glucometer (Accu-Check, Roche Diagnostics). At 15 minutes, blood was also collected for analysis of plasma insulin levels as described above.

Whole-body insulin sensitivity was assessed by an ipITT at 15 weeks post-infection. Mice were fasted for 4h, and the tests were carried out at 1:30 P.M. After an initial blood collection (*t*=0), an i.p. bolus of insulin (1 U/kg lean body mass; NOVORAPID, Novo Nordisk) was administered to the mice. Blood glucose was measured by tail bleeding at 15, 30, 60, and 90 min after insulin administration using a Glucometer.

Body composition and indirect calorimetry

Body composition was measured by MRI using an EchoMRI (Echo Medical Systems). Groups of eight mice with free access to food and water were subjected to individual indirect calorimetric measurements at 16 weeks after the start of the experiment for a period of 5 consecutive days using a Comprehensive Laboratory Animal Monitoring System (Columbus Instruments). Before the start of the measurements, the animals were acclimated to the cages and the single housing for a period of 48 h. Feeding behavior was assessed by real-time food intake. Spontaneous locomotor activity was determined by the measurement of beam breaks. Oxygen consumption and carbon dioxide production were measured at 15-min intervals. Energy expenditure and carbohydrate and fatty acid oxidation were calculated and normalized for body surface area ($kg^{0.75}$), as previously described (41).

Isolation of adipocytes and SVF from adipose tissue

Adipose tissues from the gonadal regions were collected. Two small fractions were taken for determination of adipocyte morphology and qPCR analysis, while the remainder was used for immune cell profiling by flow cytometry. For determination of adipocyte morphology, adipocytes were treated as described previously (Chapter 5, this thesis). The adipocyte size distribution, mean adipocyte diameter and volume, and adipocyte number per fat pad were calculated (42). For immune cell profiling by flow cytometry, adipose tissues were minced and digested for 1 h at 37°C in HEPES buffer (pH 7.4) containing 0.5g/l type 1 collagenase from *Clostridium histolyticum* (Sigma-Aldrich), 2% (w/v) dialyzed bovine serum albumin (BSA, fraction V, Sigma-Aldrich) and 6 mM glucose. Disaggregated adipose tissues were passed through 100 µm cell strainers which were washed with PBS supplemented with 2.5 mM EDTA and 5% FCS. After centrifugation (350 *g*, 10 minutes, room temperature), the supernatant of the filtrate was discarded and the pellet was treated with erythrocyte lysis buffer. The cells were washed once more and counted manually. Isolated SVF cells were split in two and either processed directly for the analysis of myeloid cells, or cultured for 4 hours in culture medium

in the presence of 100 ng/mL PMA, 1 µg/mL ionomycin and 10 µg/mL Brefeldin A (all Sigma-Aldrich). Following staining with the live/dead marker Aqua (Invitrogen), cells were fixed with 1.9% paraformaldehyde (Sigma-Aldrich) and stored in FACS buffer (PBS, 0.02% sodium azide, 0.5% FCS) at 4°C in the dark until subsequent analysis.

Isolation of CD45$^+$ cells from liver tissue

Livers were minced and digested for 45 minutes at 37°C in RPMI 1640 + Glutamax (Life Technologies) containing 1 mg/mL collagenase type IV from *Clostridium histolyticum*, 2000 U/mL DNase (both Sigma-Aldrich) and 1 mM $CaCl_2$. The digested liver tissues were passed through 100 µm cell strainers which were washed with PBS supplemented with 2.5 mM EDTA and 5% FCS. Following centrifugation (530 *g*, 10 minutes, 4 degrees), the supernatant of the filtrate was discarded, after which the pellet was resuspended in PBS + 2.5 mM EDTA and 5% FCS and centrifuged at 50 *g* to remove hepatocytes (3 minutes, 4 degrees). Next, supernatants were collected and pelleted (530 *g*, 10 minutes, 4 degrees). The pellet was treated with erythrocyte lysis buffer, and the cells were washed once more with PBS + 2.5 mM EDTA and 5% FCS. CD45$^+$ cells were isolated using LS columns and CD45 MicroBeads (35 µL per liver, Miltenyi Biotec) according to manufacturer's protocol. Isolated CD45$^+$ cells were counted and processed as described for the SVF.

Flow cytometry

For analysis of myeloid subsets, cells were permeabilized with 0.5% saponin (Sigma-Aldrich) in which they were also stained. Cells were incubated with an antibody against YM1 conjugated to biotin, washed, and stained with streptavidin-PerCP (BD Biosciences) and antibodies directed against CD45 (FITC), CD11b (PE-Cy7), CD11c (HV450), F4/80 (APC), Siglec-F (PE) and Ly6C (APC-Cy7). Analysis of lymphocyte subsets in CD45$^+$ cells isolated from liver was done using antibodies against CD45 (FITC), NK1.1 (PE), CD3 (APC), CD4 (PE-Cy7), CD8 (APC-Cy7), and B220 (eFluor450) diluted in FACS buffer. Finally, in PMA/ionomycin-stimulated samples, cytokine production of Th2 cells and ILCs was analysed following permeabilization as described above, using antibodies against CD11b (FITC), CD11c (FITC), GR-1 (FITC), B220 (FITC), NK1.1 (FITC), CD3 (FITC), CD4 (PerCP-eF710 or PE-Cy7), Thy1.2 (APC-eFluor780), and IL-13 (eFluor450). The stimulated CD45$^+$ cells isolated from liver were also stained for ICOS (PE-Cy7) and IL-5 (PE), while the stimulated SVF was additionally stained for CD45 (PE). Flow cytometry was performed using a FACSCanto (BD Biosciences), and gates were set according to Fluorescence Minus One (FMO) controls. Antibody information is provided in Table S2.

RNA purification and qRT-PCR

RNA was extracted from snap-frozen adipose tissue samples (~20 mg) using Tripure RNA Isolation reagent (Roche Diagnostics). Total RNA (1 µg) was reverse transcribed and quantitative real-time PCR was then performed with SYBR Green Core Kit on a MyIQ thermal cycler (Bio-Rad) using specific primers sets (available upon request). mRNA expression was normalized to RplP0 mRNA content and expressed as fold change compared to non-infected LFD-fed mice using the ΔΔCT method.

Statistical analysis

All data are presented as mean ± standard error of the mean (SEM). Statistical analysis was performed using GraphPad Prism version 6.00 for Windows (GraphPad Software, La Jolla, CA, USA) with two-tailed unpaired Student's t tests. Differences between groups were considered statistically significant at $P < 0.05$. For repeated measurements, data were analysed assuming the same scatter to increase power.

ACKNOWLEDGEMENTS

The authors thank Sander Kooijman, Patrick Rensen and Ko Willems van Dijk (LUMC) for facilitating experiments with automated metabolic cages.

REFERENCES

1. Martinez-Pomares L. The mannose receptor. *J Leukoc Biol* 2012 Dec;92(6):1177-86.
2. Everts B, et al. Schistosome-derived omega-1 drives Th2 polarization by suppressing protein synthesis following internalization by the mannose receptor. *J Exp Med* 2012 Sep 24;209(10):1753-67, S1.
3. Royer PJ, et al. The mannose receptor mediates the uptake of diverse native allergens by dendritic cells and determines allergen-induced T cell polarization through modulation of IDO activity. *J Immunol* 2010 Aug 1;185(3):1522-31.
4. Paveley RA, et al. The Mannose Receptor (CD206) is an important pattern recognition receptor (PRR) in the detection of the infective stage of the helminth Schistosoma mansoni and modulates IFNgamma production. *Int J Parasitol* 2011 Nov;41(13-14):1335-45.
5. Emara M, et al. Recognition of the major cat allergen Fel d 1 through the cysteine-rich domain of the mannose receptor determines its allergenicity. *J Biol Chem* 2011 Apr 15;286(15):13033-40.
6. Lee SJ, et al. Mannose receptor-mediated regulation of serum glycoprotein homeostasis. *Science* 2002 Mar 8;295(5561):1898-901.
7. Madsen DH, et al. M2-like macrophages are responsible for collagen degradation through a mannose receptor-mediated pathway. *J Cell Biol* 2013 Sep 16;202(6):951-66.
8. McKenzie EJ, et al. Mannose receptor expression and function define a new population of murine dendritic cells. *J Immunol* 2007 Apr 15;178(8):4975-83.
9. Linehan SA, et al. Mannose receptor and its putative ligands in normal murine lymphoid and nonlymphoid organs: In situ expression of mannose receptor by selected macrophages, endothelial cells, perivascular microglia, and mesangial cells, but not dendritic cells. *J Exp Med* 1999 Jun 21;189(12):1961-72.
10. Taylor PR, et al. The mannose receptor: linking homeostasis and immunity through sugar recognition. *Trends Immunol* 2005 Feb;26(2):104-10.
11. Mosser DM, et al. Exploring the full spectrum of macrophage activation. *Nat Rev Immunol* 2008 Dec;8(12):958-69.
12. Dalton DK, et al. Multiple defects of immune cell function in mice with disrupted interferon-gamma genes. *Science* 1993 Mar 19;259(5102):1739-42.
13. Gordon S. Alternative activation of macrophages. *Nat Rev Immunol* 2003 Jan;3(1):23-35.
14. Stein M, et al. Interleukin 4 potently enhances murine macrophage mannose receptor activity: a marker of alternative immunologic macrophage activation. *J Exp Med* 1992 Jul 1;176(1):287-92.
15. Coste A, et al. PPARgamma promotes mannose receptor gene expression in murine macrophages and contributes to the induction of this receptor by IL-13. *Immunity* 2003 Sep;19(3):329-39.
16. Odegaard JI, et al. Alternative M2 activation of Kupffer cells by PPARdelta ameliorates obesity-induced insulin resistance. *Cell Metab* 2008 Jun;7(6):496-507.
17. Chawla A, et al. Macrophage-mediated inflammation in metabolic disease. *Nat Rev Immunol* 2011 Nov;11(11):738-49.
18. Lumeng CN, et al. Obesity induces a phenotypic switch in adipose tissue macrophage polarization. *J Clin Invest* 2007 Jan;117(1):175-84.
19. Morinaga H, et al. Characterization of Distinct Subpopulations of Hepatic Macrophages in HFD/Obese Mice. *Diabetes* 2014 Oct 14;
20. Feuerer M, et al. Lean, but not obese, fat is enriched for a unique population of regulatory T cells that affect metabolic parameters. *Nat Med* 2009 Aug;15(8):930-9.
21. Mantovani A, et al. Macrophage plasticity and polarization in tissue repair and remodelling. *J Pathol* 2013 Jan;229(2):176-85.
22. Nguyen KD, et al. Alternatively activated macrophages produce catecholamines to sustain adaptive thermogenesis. *Nature* 2011 Dec 1;480(7375):104-8.
23. Qiu Y, et al. Eosinophils and type 2 cytokine signaling in macrophages orchestrate development of functional beige fat. *Cell* 2014 Jun 5;157(6):1292-308.
24. Wu D, et al. Eosinophils sustain adipose alternatively activated macrophages associated with glucose homeostasis. *Science* 2011 Apr 8;332(6026):243-7.
25. Molofsky AB, et al. Innate lymphoid type 2 cells sustain visceral adipose tissue eosinophils and

alternatively activated macrophages. *J Exp Med* 2013 Mar 11;210(3):535-49.

26. Odegaard JI, et al. Alternative macrophage activation and metabolism. *Annu Rev Pathol* 2011;6:275-97.
27. Movita D, et al. Kupffer cells express a unique combination of phenotypic and functional characteristics compared with splenic and peritoneal macrophages. *J Leukoc Biol* 2012 Oct;92(4):723-33.
28. Canton J, et al. Scavenger receptors in homeostasis and immunity. *Nat Rev Immunol* 2013 Sep;13(9):621-34.
29. Gazi U, et al. Influence of the mannose receptor in host immune responses. *Immunobiology* 2009;214(7):554-61.
30. Regnier-Vigouroux A. The mannose receptor in the brain. *Int Rev Cytol* 2003;226:321-42.
31. Thaler JP, et al. Minireview: Inflammation and obesity pathogenesis: the hypothalamus heats up. *Endocrinology* 2010 Sep;151(9):4109-15.
32. Thaler JP, et al. Obesity is associated with hypothalamic injury in rodents and humans. *J Clin Invest* 2012 Jan 3;122(1):153-62.
33. Andersson U, et al. Neural reflexes in inflammation and immunity. *J Exp Med* 2012 Jun 4;209(6):1057-68.
34. Wang L, et al. Pten deletion in RIP-Cre neurons protects against type 2 diabetes by activating the anti-inflammatory reflex. *Nat Med* 2014 May;20(5):484-92.
35. Cani PD, et al. Metabolic endotoxemia initiates obesity and insulin resistance. *Diabetes* 2007 Jul;56(7):1761-72.
36. Schipper HS, et al. Adipose tissue-resident immune cells: key players in immunometabolism. *Trends Endocrinol Metab* 2012 Aug;23(8):407-15.
37. Marttila-Ichihara F, et al. Macrophage mannose receptor on lymphatics controls cell trafficking. *Blood* 2008 Jul 1;112(1):64-72.
38. Elvevold K, et al. Liver sinusoidal endothelial cells depend on mannose receptor-mediated recruitment of lysosomal enzymes for normal degradation capacity. *Hepatology* 2008 Dec;48(6):2007-15.
39. Malovic I, et al. The mannose receptor on murine liver sinusoidal endothelial cells is the main denatured collagen clearance receptor. *Hepatology* 2007 Jun;45(6):1454-61.
40. Jansen KM, et al. Mannose receptor regulates myoblast motility and muscle growth. *J Cell Biol* 2006 Jul 31;174(3):403-13.
41. van den Berg SA, et al. High levels of dietary stearate promote adiposity and deteriorate hepatic insulin sensitivity. *Nutr Metab (Lond)* 2010;7:24.
42. Jo J, et al. Hypertrophy and/or Hyperplasia: Dynamics of Adipose Tissue Growth. *PLoS Comput Biol* 2009 Mar;5(3):e1000324.

SUPPLEMENTAL DATA

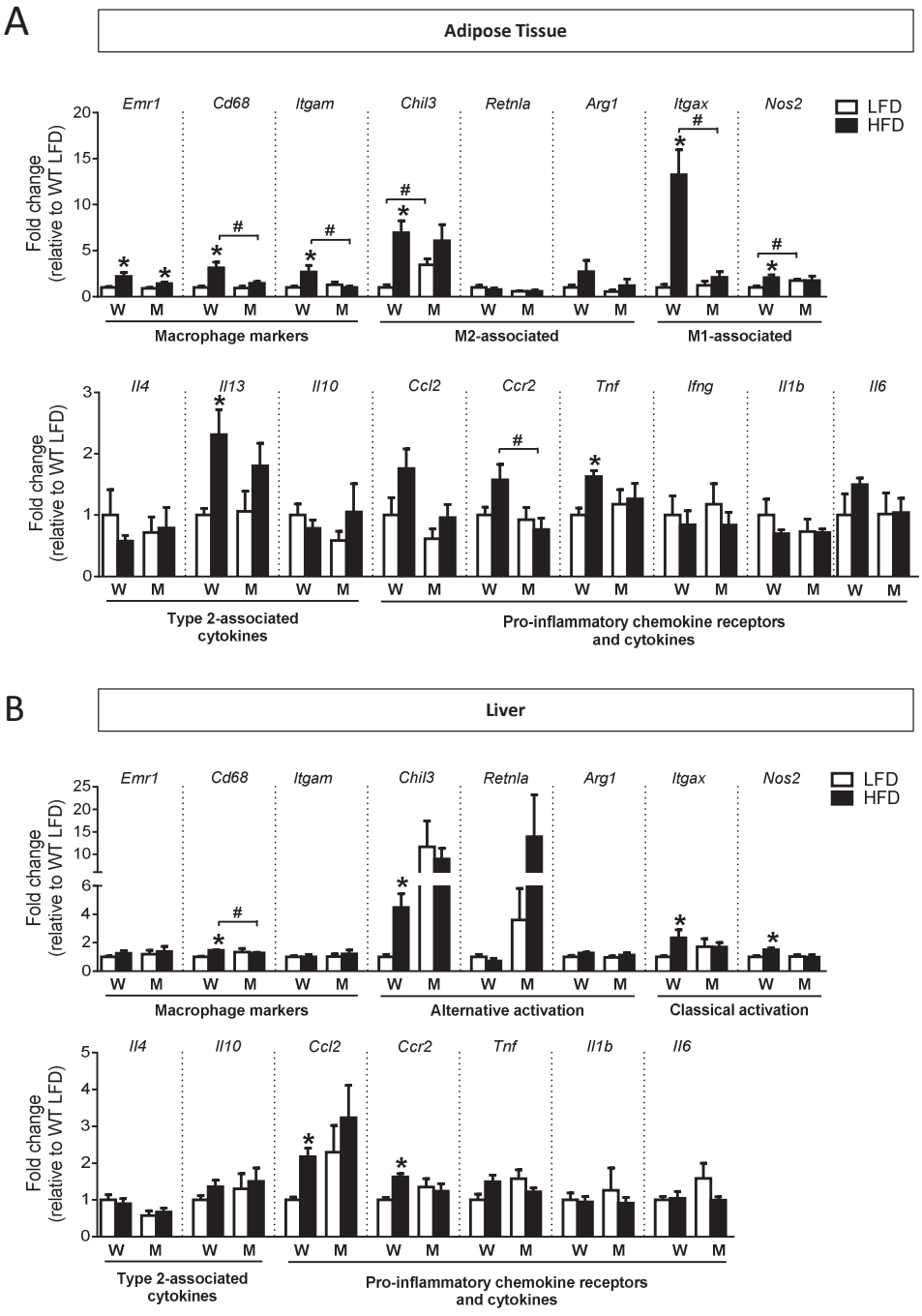

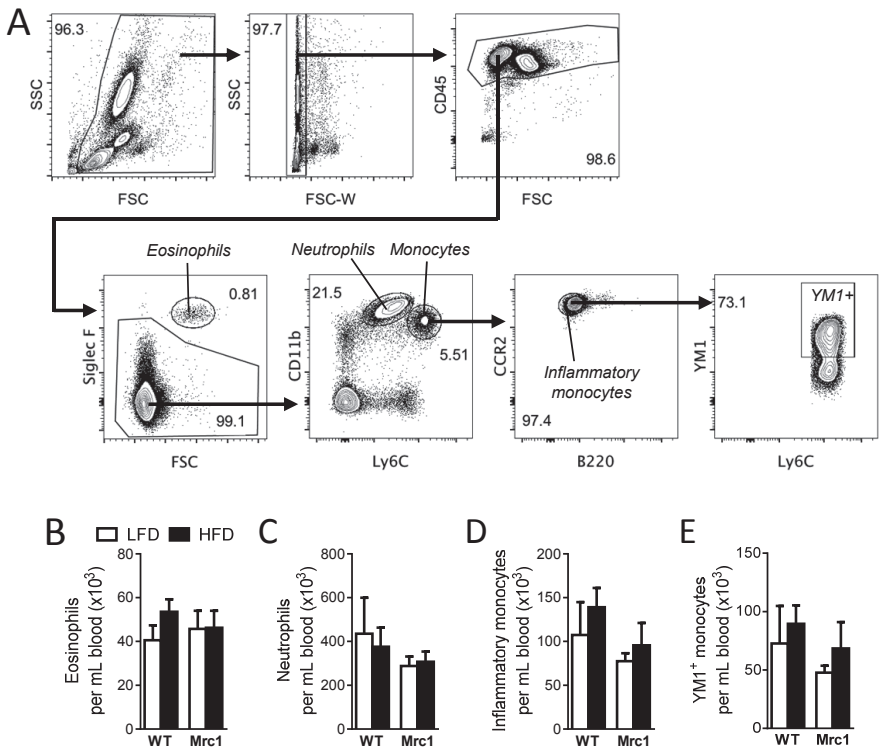

Figure S2. Diet and genotype do not affect myeloid cells in blood. Wild-type (WT) and MR-deficient (Mrc1) mice were fed a LFD or HFD for 18 weeks. At sacrifice, blood was collected and fixed using Lyse/Fix buffer (BD Biosciences). Blood cells were counted, stained and analyzed by flow cytometry. The gating strategy is shown for eosinophils, neutrophils, monocytes, inflammatory monocytes, and YM1$^+$ inflammatory monocytes (A). The numbers of eosinophils (B), neutrophils (C), inflammatory monocytes (D) and YM1$^+$ inflammatory monocytes (E) per mL blood were determined. Results are expressed as means ± SEM. * P<0.05 HFD *vs* LFD, # P<0.05 WT *vs* Mrc1 (n = 10-15 animals per group).

◀ **Figure S1. Analysis of inflammatory markers in adipose tissue and liver by qPCR.** Wild-type (WT) and MR-deficient (Mrc1) mice were fed a LFD or HFD for 18 weeks. At sacrifice gonadal WAT and liver tissues were collected and immediately snap-frozen. mRNA expression of the indicated genes in gonadal WAT (A) and liver (B) was quantified by RT-PCR relative to RplP0 gene and expressed as fold difference compared to the LFD-fed mice. Primer sequences are provided on request. Results are expressed as means ± SEM. * P<0.05 HFD *vs* LFD, # P<0.05 WT *vs* Mrc1 (n = 4-6 animals per group). Genes encode the following proteins: F4/80 (*Emr1)*; CD68 (*CD68*); CD11b (*Itgam*); YM1 (*Chil3*); FIZZ1 (*Retnla*); Arginase-1 (*Arg1*); CD11c (*Itgax*); iNOS (*Nos2*); IL-4 (*Il4*); IL-13 (*Il13*); IL-10 (*Il10*); MCP-1 (*Ccl2*); CCR-2 (*Ccr2*); TNF-α (*Tnf*); IFN-γ (*Ifng*); IL-1β (*Il1b*); IL-6 (*Il6*).

Table S1. Baseline characteristics of WT and MR-deficient mice.

	WT	Mrc1	P-value
Body weight	27.04 ± 0.39	26.12 ± 0.43	0.12
Lean mass	25.27 ± 0.39	24.43 ± 0.42	0.15
Fat mass	1.28 ± 0.10	1.11 ± 0.08	0.18
Glucose	8.78 ± 0.20	8.45 ± 0.27	0.33
Insulin	0.49 ± 0.04	0.38 ± 0.04	0.07
Total Cholesterol	2.56 ± 0.06	2.79 ± 0.07	**0.03**
Triglycerides	0.54 ± 0.02	0.50 ± 0.02	0.21

Baseline characteristics of wild-type (WT) and MR-deficient (Mrc1) mice were determined at the start of the experiment. Body weight and body composition are shown, and plasma glucose, insulin, total cholesterol and triglyceride levels in 4h-fasted mice. Results are expressed as means ± SEM (n = 25 for WT and 22 for Mrc1).

Table S2. Antibody information.

Target	Clone	Conjugate	Manufacturer
B220	RA3-6B2	eFluor450	eBioscience
B220	RA3-6B2	FITC	eBioscience
CD3	17A2	APC	eBioscience
CD3	17A2	FITC	eBioscience
CD4	GK1.5	PE-Cy7	eBioscience
CD4	GK1.5	PerCP-eF710	eBioscience
CD8a	53-6.7	APC-Cy7	Biolegend
CD11b	M1/70	PE-Cy7	eBioscience
CD11b	M1/70	FITC	eBioscience
CD11c	HL3	Horizon V450	BD Biosciences
CD11c	HL3	FITC	BD Biosciences
CD45.2	104	FITC	Biolegend
CD45.2	104	PE	Biolegend
F4/80	BM8	APC	eBioscience
GR-1	RB6-8C5	FITC	BD Biosciences
IL-5	TRFK5	PE	Biolegend
IL-13	eBio13A	eFluor450	eBioscience
ICOS	C398.4A	PE-Cy7	Biolegend
Ly-6C	HK1.4	APC-Cy7	Biolegend
NK1.1	PK136	PE	BD Biosciences
NK1.1	PK136	FITC	eBioscience
Siglec-F	E50-2440	PE	BD Biosciences
Thy1.2	52-2.1	APC-eFluor780	eBioscience